Journal of Quantitative Spectroscopy & Radiative Transfer 150 (2015) 68–75

Contents lists available at ScienceDirect

Journal of Quantitative Spectroscopy & Radiative Transfer

journal homepage: www.elsevier.com/locate/jqsrt

Mixing rules and morphology dependence of the scatterer

Gorden Videen [a,b,*], Evgenij Zubko [c], Wenbo Sun [d], Yuriy Shkuratov [c], Alex Yuffa [a]

[a] Army Research Laboratory, Adelphi, MD 20783, USA
[b] Space Science Institute, Boulder, CO 80301, USA
[c] Institute of Astronomy, V.N. Karazin Kharkiv National University, 35 Sumskaya Street, Kharkiv 61022, Ukraine
[d] Science Systems and Applications Inc., Hampton, VA 23666, USA

ARTICLE INFO

Article history:
Received 12 May 2014
Received in revised form
23 July 2014
Accepted 26 July 2014
Available online 8 August 2014

Keywords:
Bruggeman
Mixing rules
Morphology
Agglomerate
Agglomerated debris
Light scattering

ABSTRACT

We use the discrete dipole algorithm (DDA) to calculate the light-scattering properties from arbitrarily shaped, heterogeneous agglomerated debris particles to study the performance of effective medium approximations. The homogenization of the material properties of the particle has little effect on the orientation-averaged intensity phase function. However, there are some differences in the polarization response. While the structure of the linear-polarization response is not significantly different between the homogeneous and heterogeneous cases, the amplitude of the polarization tends to show a dependence on particle heterogeneity. The Bruggeman mixing rule tends to reproduce the heterogeneous results marginally better than using the average of two distributions of the individual homogeneous components. In addition to the irregularly shaped particles, we also calculated scattering properties of equivalent-volume, homogeneous spheres. As expected, the errors due to assuming homogeneous particles are overwhelmed by those introduced by assuming the irregularly shaped particle may be replaced by an equivalent spherical particle.

Published by Elsevier Ltd.

1. Introduction

Effective medium theories (EMTs), or mixing rules, provide a means of calculating light scattering properties of heterogeneous particles by assuming they are homogeneous. The most frequently used one is the Bruggeman mixing rule. In the context of light-scattering, mixing rules rose to prominence in the wake of the studies of morphology dependent resonances (MDRs) in the 1980s and 1990s. While very few of these early studies actually considered the effect of morphology, a number of them did consider the effect of heterogeneities on the resulting resonances [1–6]. It was impossible to verify the results theoretically at that time, but one significant experimental effort resulted in the production of a composite particle that could be measured in the microwave region [7], and whose results could also be compared with Lorenz–Mie results calculated using the Bruggeman and Maxwell–Garnett mixing rules. In the mid-1990s, models to calculate light-scattering from a sphere containing an inclusion were developed [8,9], and it became practical to make some verification of mixing rules using the approximation that a single inclusion is present [10–12]. In these studies the size of the inclusion was increased beyond that of a Rayleigh particle to address Bohren's concerns [13] about extended effective medium approximations previously proposed by Chýlek and Srivastava [14]. The primary application at the time was to address anomalous absorption observed from clouds, that was hypothesized to result from absorbing nucleating particles in water droplets, the so-called cloud-absorption anomaly [15–17].

It was not until recently that a test of mixing rules was performed using a model spherical droplet containing a

* Corresponding author. Tel.: +1 301 394 1871.
E-mail address: gorden.w.videen.civ@mail.mil (G. Videen).

http://dx.doi.org/10.1016/j.jqsrt.2014.07.022
0022-4073/Published by Elsevier Ltd.

large number of small inclusions. Mishchenko, Liu and Mackowski use a new formulation of the superposition *T*-matrix algorithm for a spherical volume filled with a large number of inclusions [18] whose roots go back some 20 years [19,20]. More recently, Mishchenko, Dlugach, and Zakharova used this model to validate the concept of an unrestricted effective-medium approximation [21]. Unlike previous examinations, the researchers were finally equipped with efficient algorithms and the necessary computational resources to perform legitimate tests. In the spirit of the initial studies, the authors considered the effect of inclusions on resonances in their tests. While they found that the mixing rules largely failed to predict the resonance behavior, except in gross qualitative ways, i.e. they do appear to predict the direction of resonance shifts, these particular simulations do represent an extremely difficult test as the inclusions represent secondary scattering sites that scatter energy from the spherical cavity, the physics of which cannot be contained within a model of simple Lorenz–Mie theory using a mixing rule.

Within the last decade, it has become practical to use numerical techniques, like the discrete dipole approximation (DDA) to calculate the light-scattering properties from arbitrarily shaped, heterogeneous particles. Such particles include mixed-phase aerosols, ice, mineral dust, etc., and have numerous remote-sensing applications. From a practical standpoint, the use of EMTs to approximate the optical properties of such particles presents a tremendous cost-savings in computational time because the number of different material combinations of such a class of particles is infinite. In this manuscript we consider heterogeneous, irregularly shaped ice particles and perform comparisons of the resulting light-scattering properties with those of identically shaped, but homogeneous particles using two simple mixing rules.

2. Heterogeneous particles

We employ the DDA to calculate the light-scattering properties of heterogeneous agglomerated debris particles.

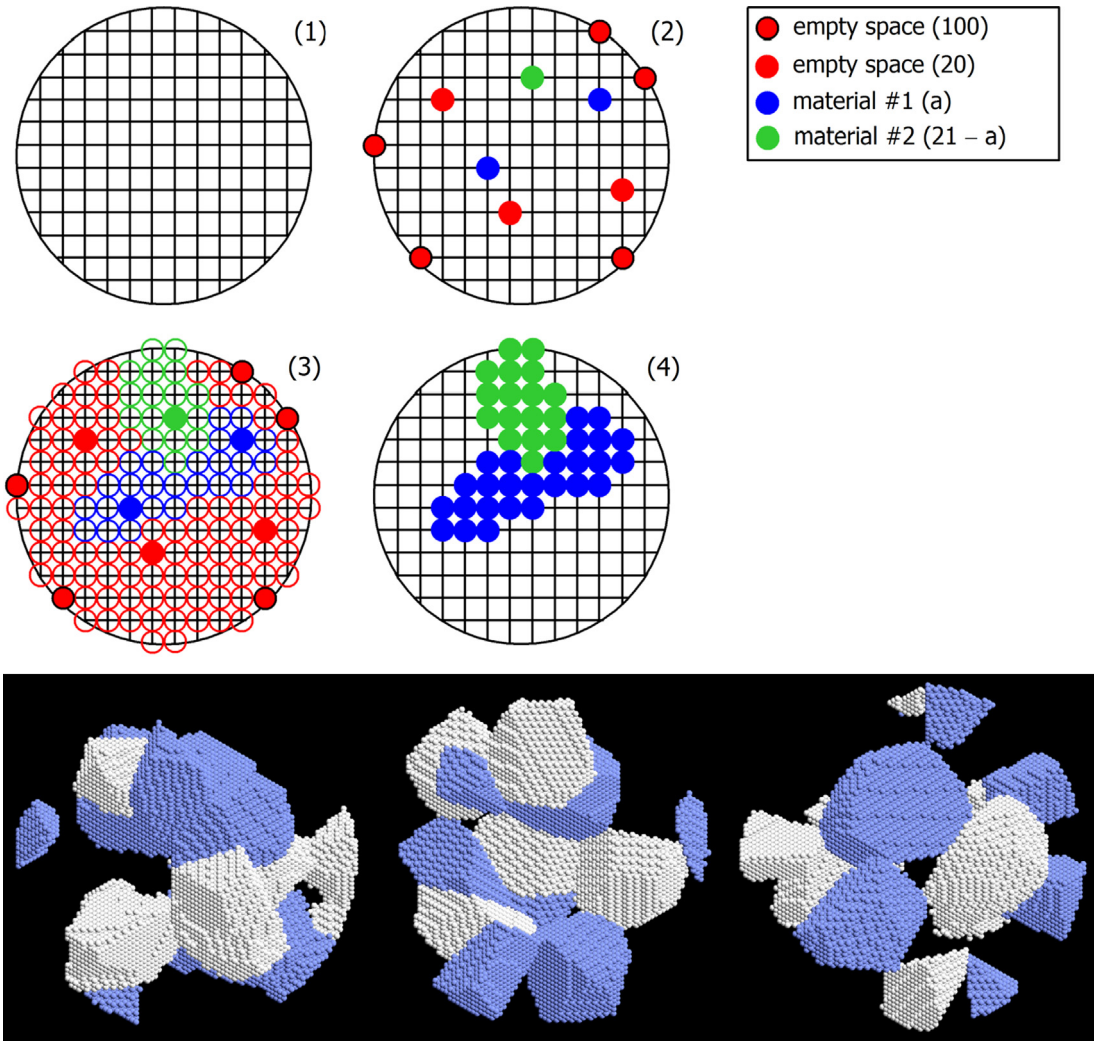

Fig. 1. A cartoon depicting the method for generating heterogeneous agglomerated debris particles in two dimensions (top) and three example images of agglomerated debris particles (bottom).

Since its introduction in 1973 [22], the DDA has undergone several improvements to increase the efficiency. Most notable have been the incorporation of fast Fourier transform (FFT) algorithms [23] and the lattice dispersion relation [24]. The code used in this study was based on a code developed in 2003 [25] that has been tested with other implementations of the DDA [26].

The DDA is extremely flexible and does not require an analytical description of the particles. The only particle specification required is the polarizabilities on a three-dimensional grid that correspond to those of the particle in real space. We have developed several different types of morphologies of irregularly shaped particles and examined their resulting properties (see, for example, [27–29]). In these simulations, we consider the agglomerated debris particles.

The generation of heterogeneous agglomerated debris particles within the DDA construct is shown in Fig. 1. For visualization, this illustration is shown in two-dimensions. The extension to three dimensions is obvious. We consider a spherical volume that is filled with a cubic lattice. The radius of sphere is chosen to be 32 cubic cells, so the sphere consists

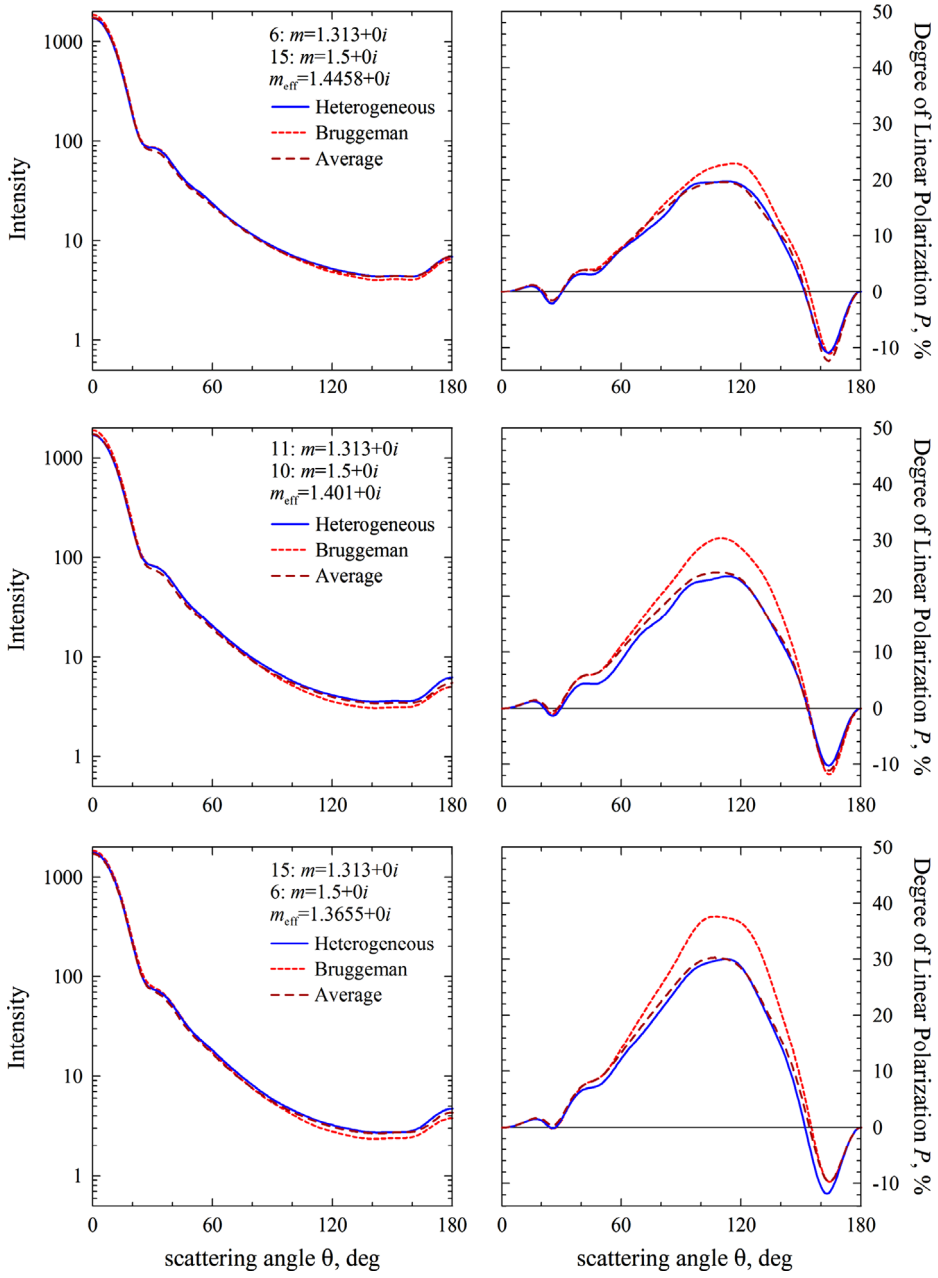

Fig. 2. Light-scattering intensity (left) and polarization (right) from $x=10$ heterogeneous, orientation-averaged agglomerated debris particles composed using 21 seed cells: 6 of $m=1.313+0i$ and 15 of $m=1.5+0i$, having $m_{\text{eff}}=1.446+0i$ (top); 11 of $m=1.313+0i$ and 10 of $m=1.5+0i$, having $m_{\text{eff}}=1.4+0i$ (middle); and 15 of $m=1.313+0i$ and 6 of $m=1.5+0i$, having $m_{\text{eff}}=1.3655+0i$ (bottom).

of 137,376 cells. The outermost cells forming this initial matrix belong to a surface layer, whose depth is 0.5% of the sphere radius. Note in a cubic lattice, dipoles forming the boundary of the target have less than 26 neighbor cells. In the case of the 137,376-cell sphere, there are a total of 18,608 boundary cells. We measure the depth of the surface layer from the sphere boundary. The small depth chosen for agglomerated debris particles implies that the surface layer coincides with the boundary layer, i.e., it also consists of 18,608 cells. Of these surface cells, 100 are randomly chosen to be seed cells of empty space. These surface cells ensure that the particle exterior is irregular. Within the interior, we randomly select 21 seed cells of material and 20 seed cells of empty space. The material seed cells may represent one or more different types of materials. Finally, each cell within the matrix is designated as having the optical properties of the nearest seed cell. Images of sample agglomerated debris particles are shown in the lower panels of Fig. 1.

In this study, we consider particles consisting of two different types of material seed cells. Due to its abundant applications, one of these materials is chosen to be water-ice, having a refractive index $m=1.313+0i$ [30]. Irregularly

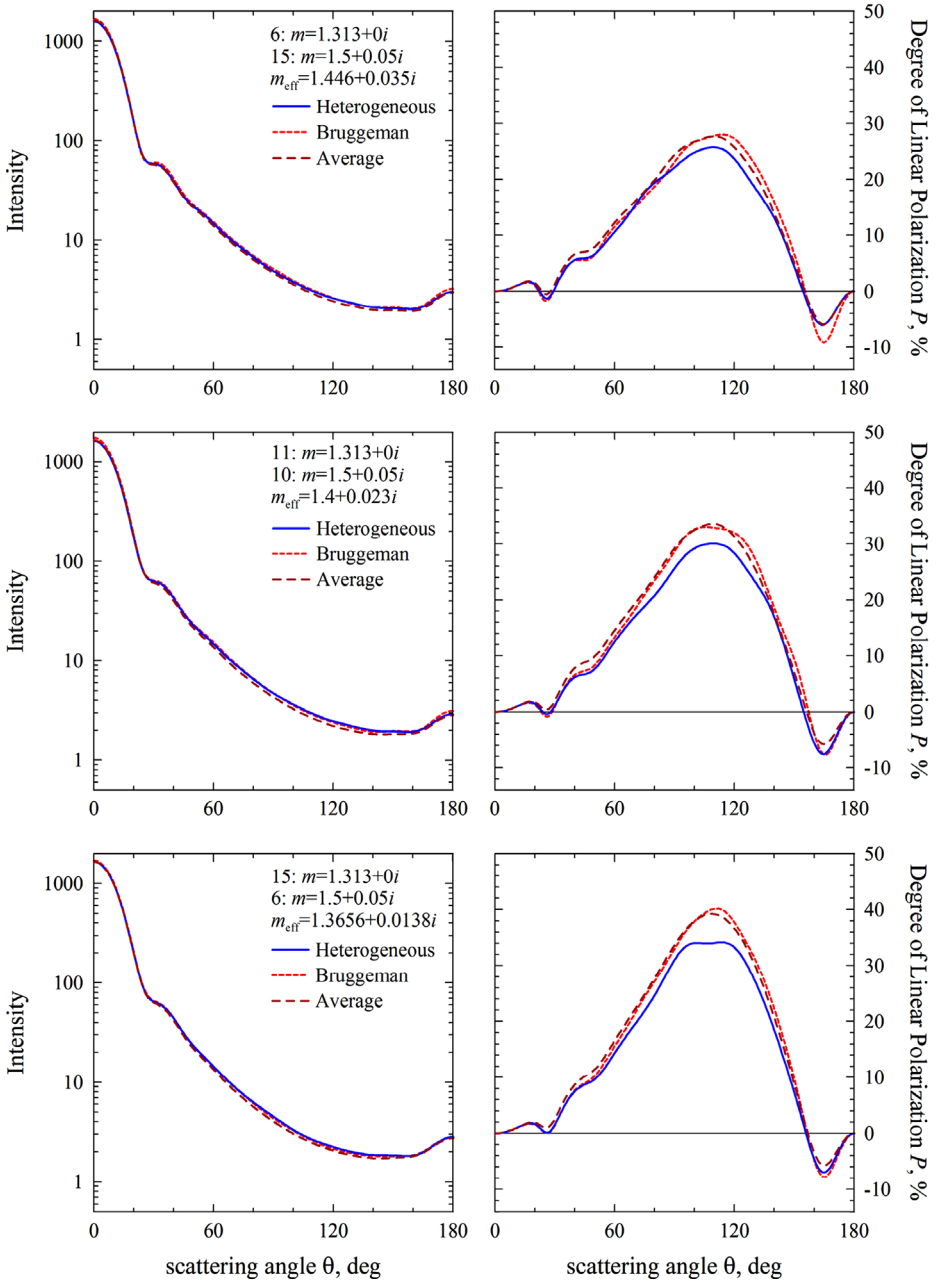

Fig. 3. Light-scattering intensity (left) and polarization (right) from $x=10$ heterogeneous, orientation-averaged agglomerated debris particles composed using 21 seed cells: 6 of $m=1.313+0i$ and 15 of $m=1.5+0.05i$, having $m_{\text{eff}}=1.446+0.035i$ (top); 11 of $m=1.313+0i$ and 10 of $m=1.5+0.05i$, having $m_{\text{eff}}=1.4+0.023i$ (middle); and 15 of $m=1.313+0i$ and 6 of $m=1.5+0.05i$, having $m_{\text{eff}}=1.3656+0.0138i$ (bottom).

shaped ice particles are a common target in remote-sensing studies of planetary atmospheres [31–33] and in comets [34–39]. In the atmosphere, water often forms around some nucleating particles of different materials. We consider three different types of material to mix with the ice: (1) highly absorbing, corresponding to carbon and having $m=2.43+0.59i$ [40]; (2) moderately absorbing, equally corresponding to organic material or Mg–Fe silicates and having $m=1.5+0.05i$ [41,42]; and (3) non-absorbing, corresponding to Mg-rich Fe-poor silicates and having $m=1.5+0i$ [42]. These present different cases for testing effective medium theories.

In addition to the results from heterogeneous particles calculated using the DDA from the particles constructed using the method outlined in Fig. 1 (designated "Heterogeneous"), we consider two basic mixing rules. We consider a homogeneous particle whose refractive index is calculated using the Bruggeman mixing rule (designated "Bruggeman"). We also consider the volume-averaged light-scattering properties assuming a mixture of homogeneous particles having the refractive indices of the two individual components that make up the heterogeneous particles (designated "Average"). These three different particles have exactly the same morphology, but vary in their distribution of refractive index.

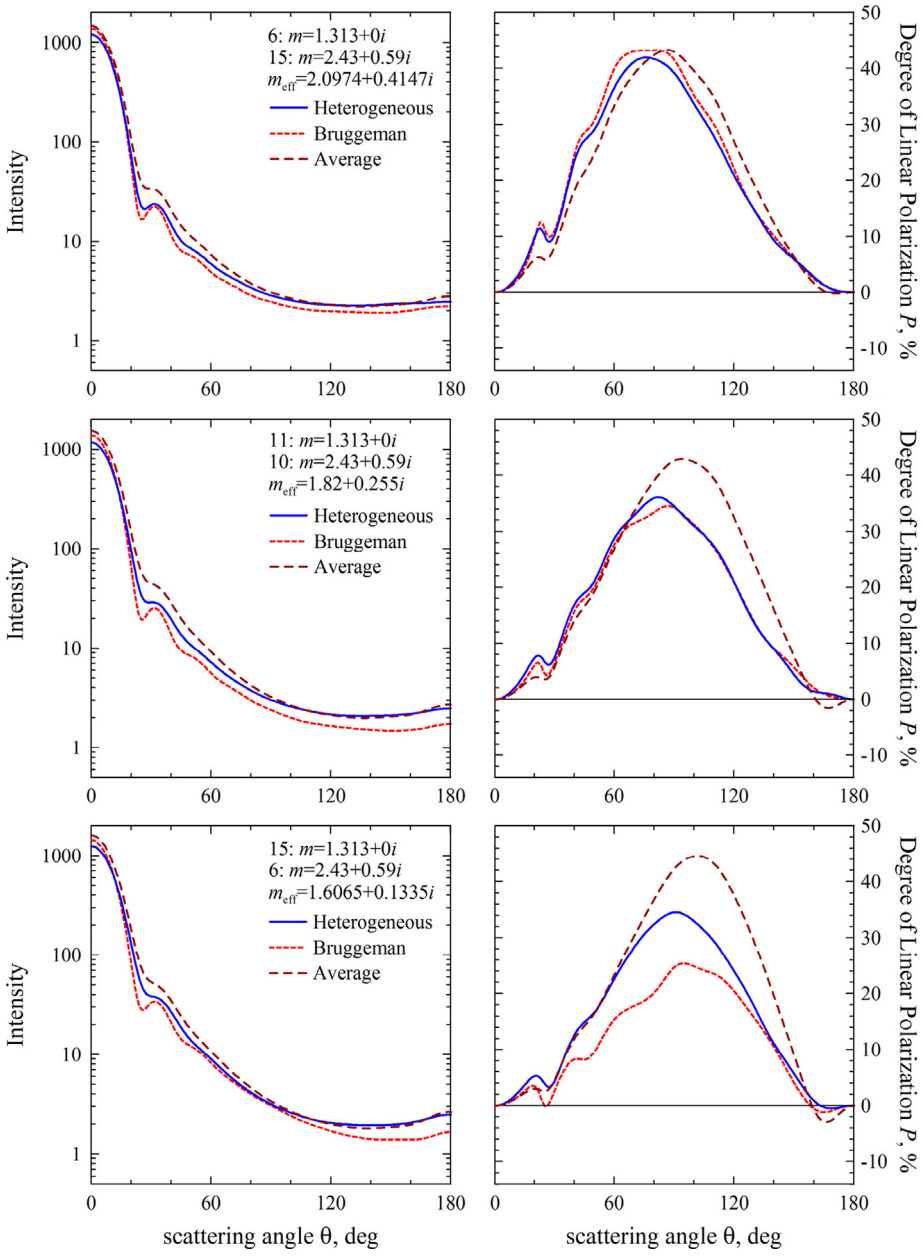

Fig. 4. Light-scattering intensity (left) and polarization (right) from $x=10$ heterogeneous, orientation-averaged agglomerated debris particles composed using 21 seed cells: 6 of $m=1.313+0i$ and 15 of $m=2.43+0.59i$, having $m_{\text{eff}}=2.0974+0.4147i$ (top); 11 of $m=1.313+0i$ and 10 of $m=2.43+0.59i$, having $m_{\text{eff}}=1.82+0.255i$ (middle); and 15 of $m=1.313+0i$ and 6 of $m=2.43+0.59i$, having $m_{\text{eff}}=1.6065+0.1335i$ (bottom).

3. Results

In many remote-sensing applications, the particle orientation is unknown and usually it has no known preferential orientation. In addition, particles are not identical, so the signal measured is an average signal over both particle orientation and configuration morphology. To perform averaging over the model particles, we consider a minimum of 500 model particles having size parameter $x=2\pi r/\lambda=10$, where r is the radius of the initial spherical volume filled with the cubic lattice and λ is the wavelength of the incident radiation. The light scattering is computed from each sample in a single orientation, and is averaged over 100 scattering planes that are evenly distributed around the direction of propagation of the incident light. Averaging is continued until the standard deviation of the linear polarization over the entire range of scattering angle θ does not exceed 1%. Typically, this requires significantly more than 500 sample particles.

In Figs. 2–4 we show the resulting light-scattering intensity phase functions ($\propto M_{11}$) and corresponding linear-polarization response (Mueller matrix element $-M_{21}/M_{11}$) as a function of scattering angle θ for different concentrations of materials. In the top row, the ice makes up the lowest material concentration of the agglomerates, approximately 25%. In the middle rows, the ice makes up about 50% of the material and in the bottom rows, the ice makes up about 75% of the material concentration.

Accompanying the ice in the agglomerates of Fig. 2 is a non-absorbing material having refractive index $m=1.5+0i$ that may correspond with a silicate in the visible. We begin with a completely non-absorbing particle primarily for illustrative purposes, but such mixed material could correspond with silicates embedded in an ice matrix that may occur in cometary coma, for instance. In all the examples we show, the intensity phase functions (left column) have very similar shape. A large forward-scattering peak drops nearly two orders to a minimum at approximately $\theta=20^\circ$. This is the primary diffraction minimum and it is visible because of the high level of size mono-dispersity in our samples. This is followed by a small peak and then a much slower decay of another order. Beginning at $\theta\sim150^\circ$ is the backscattering intensity surge. The curves for the Heterogeneous, Bruggeman and Average particles are nearly coincident. Differences are only apparent when examining the gross scattering properties of Table 1. For these particular material parameters, the differences are on the order of a few percent. The agreement of the Heterogeneous particles with the Average particles is slightly better than with those calculated using the Bruggeman mixing rule.

The linear-polarization response seen in the right column of Fig. 2 shows a positive branch that peaks at ~30–40% when scattering angle $\theta\sim110^\circ$. While the different particles all produce the same general shape, the agreement with the Heterogeneous particles again is slightly better with the Average particles. One other common feature of the polarization is the negative branch that occurs in the backscatter region. This negative polarization feature is prominent for this somewhat monodisperse system, extending to approximately −11%. The depth and position do not vary significantly between the systems.

In Fig. 3, we have incorporated some relatively small amount of absorption to the material accompanying the ice: $m=1.5+0.05i$. Again the total-intensity phase functions of the three different particle systems are nearly coincident and the gross scattering properties remain in agreement. In this case the Bruggeman mixing rule outperforms the particle averaging. The linear-polarization also remains in good agreement for the different systems, although the positive polarization maximum of the heterogeneous system is slightly less than the homogeneous systems (Table 2).

We next consider an extreme case. Accompanying the ice in the agglomerates of Fig. 4 is a highly refractive and absorbing material having refractive index $m=2.43+0.59i$ that corresponds with carbon in the visible. Such mixed material would be applicable for cirrus clouds, for instance. The intensity phase functions (left column) all have very similar shape, but they are no longer coincident. We also note that the backscattering intensity surge is weaker and broader, giving the phase function a more parabolic shape.

While the curves have similar shapes, there are subtle differences. The intensities of the Average particles are greater than the Heterogeneous particles, which are in turn greater than the Bruggeman particles (see Table 3). This is not surprising, and was seen in previous studies of spherical host particles [10–12]. It is easiest for waves to

Table 1
Integral light-scattering characteristics of agglomerated debris particles composed of water ice ($m=1.313+0i$) and silicates ($m=1.5+0i$).

Mode	Q_{ext}	Q_{abs}	Q_{sca}	g	SSA	A
6 Seed cells $m=1.313+0i$ and 15 seed cells $m=1.5+0i$						
Heterogeneous	2.550	0	2.550	0.752	1	0.113
Bruggeman	2.652	0	2.652	0.768	1	0.107
Average	2.529	0	2.529	0.758	1	0.114
11 Seed cells $m=1.313+0i$ and 10 seed cells $m=1.5+0i$						
Heterogeneous	2.494	0	2.494	0.779	1	0.102
Bruggeman	2.635	0	2.635	0.803	1	0.082
Average	2.445	0	2.445	0.788	1	0.090
15 Seed cells $m=1.313+0i$ and 6 seed cells $m=1.5+0i$						
Heterogeneous	2.457	0	2.457	0.809	1	0.077
Bruggeman	2.551	0	2.551	0.826	1	0.062
Average	2.378	0	2.378	0.813	1	0.072

Table 2
Integral light-scattering characteristics of agglomerated debris particles composed of water ice ($m=1.313+0i$) and organics ($m=1.5+0.05i$).

Mode	Q_{ext}	Q_{abs}	Q_{sca}	g	SSA	A
6 Seed cells $m=1.313+0i$ and 15 seed cells $m=1.5+0.05i$						
Heterogeneous	2.457	0.461	1.995	0.814	0.812	0.0492
Bruggeman	2.543	0.472	2.071	0.816	0.814	0.0530
Average	2.441	0.442	1.999	0.822	0.819	0.0485
11 Seed cells $m=1.313+0i$ and 10 seed cells $m=1.5+0.05i$						
Heterogeneous	2.436	0.332	2.104	0.823	0.864	0.0475
Bruggeman	2.542	0.328	2.214	0.830	0.871	0.0515
Average	2.386	0.295	2.092	0.834	0.877	0.0464
15 Seed cells $m=1.313+0i$ and 6 seed cells $m=1.5+0.05i$						
Heterogeneous	2.414	0.210	2.204	0.835	0.913	0.0461
Bruggeman	2.452	0.202	2.249	0.839	0.918	0.0457
Average	2.343	0.177	2.166	0.842	0.925	0.0446

penetrate the homogeneous Bruggeman particles and become absorbed, and more difficult for waves to penetrate the homogeneous $m=2.43+0.59i$ particles that provide the absorption for the Average case. Unlike those previous studies in which the increased absorption was compensated by a decreased amount of scattering, we do not necessarily see this trend in the data of Table 1. This likely is the result of the destruction of the resonance features because these particles are far from being spherical. The resulting extinction of the heterogeneous particles is significantly different from those of the homogeneous particles. These differences appear to increase when the volume ratio of the absorbing component decreases. While this could have a significant impact in atmospheric remote sensing where cirrus may contain a small amount of highly absorbing material, we note that the concentrations of absorbing component in these examples is much higher than is typically experienced in real cirrus. For the much smaller concentrations as would be typically found ($<1\%$), our simulations have shown almost no difference when a homogeneous-particle approximation is used.

The linear-polarization response seen in the right column of Fig. 4 shows a positive branch that peaks at $\sim 40\%$ when scattering angle $\theta \sim 80^\circ$. We note that the absorption has increased the magnitude and shifted it toward the forward scattering [27]. While the different mixing rules all reproduce the same general shape, the relative amplitudes of the polarization depend on the concentration of absorbing material. The amplitude for the Average system tends to remain about the same, but decreases for the Heterogeneous and Bruggeman systems. One other common feature of the polarization is the negative branch that occurs in the backscatter region. However, the negative branch does not exist when absorption is high [26], so it does not exist for these Bruggeman and Heterogeneous particles and only exists in the non-absorbing component of the Average particles.

Finally, we note that in many applications (see, for instance, [43–45]), equivalent homogeneous spheres are used to calculate the scattering properties of irregularly shaped, heterogeneous particles. In Fig. 5, we show the total intensity and linear-polarization responses for particles containing nearly equal components of $m=2.43+0.59i$ and $m=1.313+0i$ material. As in previous studies, it is apparent that such an approximation does a poor job of reproducing the actual optical properties. It should be noted that Chýlek, Grams and Pinnick proposed a modification to Lorenz–Mie theory to address the effects of non-spherical particles in a manner that may be considered similar to effective medium theories [46].

Table 3
Integral light-scattering characteristics of agglomerated debris particles composed of water ice ($m=1.313+0i$) and amorphous carbon ($m=2.43+0.59i$).

Mode	Q_{ext}	Q_{abs}	Q_{sca}	g	SSA	A
6 Seed cells $m=1.313+0i$ and 15 seed cells $m=2.43+0.59i$						
Heterogeneous	2.238	1.046	1.192	0.813	0.533	0.0401
Bruggeman	2.408	1.209	1.199	0.841	0.498	0.0363
Average	2.367	0.850	1.517	0.834	0.641	0.0456
11 Seed cells $m=1.313+0i$ and 10 seed cells $m=2.43+0.59i$						
Heterogeneous	2.166	0.860	1.306	0.817	0.603	0.0405
Bruggeman	2.418	1.172	1.246	0.852	0.515	0.0283
Average	2.337	0.567	1.770	0.843	0.758	0.0444
15 Seed cells $m=1.313+0i$ and 6 seed cells $m=2.43+0.59i$						
Heterogeneous	2.149	0.626	1.523	0.827	0.709	0.0406
Bruggeman	2.438	1.015	1.423	0.842	0.584	0.0273
Average	2.313	0.340	1.973	0.848	0.853	0.0435

4. Conclusion

In this study we have examined the use of mixing rules to approximate the light-scattering properties of irregularly shaped, heterogeneous particles. Our studies suggest that mixing rules can do an adequate job of reproducing the total-intensity phase function and the linear-polarization response in the cases where there is moderate difference between refractive indices of the constituent species. We note that the angular profile of the linear polarization is more sensitive to heterogeneous composition of target particles. Nevertheless, the variance of the polarimetric response with composition does not suggest systematic differences in

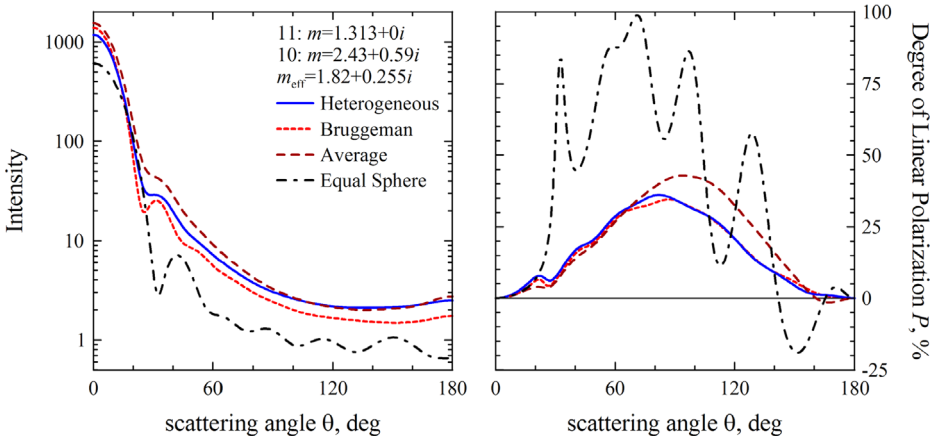

Fig. 5. Light-scattering intensity (left) and polarization (right) from $x=10$ heterogeneous, orientation-averaged agglomerated debris particles composed using 21 seed cells: 11 of $m=1.313+0i$ and 10 of $m=2.43+0.59i$, having $m_{eff}=1.82+0.255i$ as shown in the middle row of Fig. 2. Superimposed are the light-scattering responses of a homogeneous volume-equivalent sphere calculated using m_{eff}.

behavior, but the amplitude differences in positive polarization, for instance, may have an impact on the accuracy of parameters retrieved from photo-polarimetric measurements. The mixing rule may provide a satisfactory accuracy even when the differences in refractive index of the individual components are extreme. Finally, we note that the light-scattering response in heterogeneous particles can be reasonably well estimated from averaging of light-scattering responses in homogeneous particles, which are composed of given constituent materials and volume ratio. Accuracy of this approach is comparable to that in the Bruggeman mixing rule. One significant advantage of this approach is that, once computations of the light scattering from individual homogeneous particles are made, estimations of light-scattering properties of particles having different volume ratios can be made at almost no additional cost.

Acknowledgments

This work was supported by NASA Glory fund 09-GLORY09-0027. Wenbo Sun also was supported by NASA CLARREO mission and he thanks Bruce A. Wielicki and Rosemary R. Baize for this support.

References

[1] Chýlek P, Ngo D, Pinnick RG. Resonance structure of composite and slightly absorbing spheres. J Opt Soc Am A 1992;9:775–80.
[2] Mazumder M, Hill SC, Barber PW. Morphology-dependent resonances in inhomogeneous spheres: comparison of the layered T-matrix method and the time-independent perturbation method. J Opt Soc Am A 1992;9:1844.
[3] Gu J, Ruekgauer TE, Xie J-G, Armstrong RL. Effect of particulate seeding on microdroplet angular scattering. Opt Lett 1993;18:1293–5.
[4] Bronk BV, Smith MJ, Arnold S. Photon-correlation spectroscopy for small spherical inclusions in a micrometer-sized electrodynamically levitated droplet. Opt Lett 1993;18:93.
[5] Lin H-B, Huston AL, Eversole JD, Campillo AJ, Chýlek P. Internal scattering effects on microdroplet resonant emission structure. Opt Lett 1992;17:970–2.
[6] Ngo D, Pinnick RG. Suppression of scattering resonances in inhomogeneous microdroplets. J Opt Soc Am A 1994;11:1352–9.
[7] Chýlek P, Srivastava V, Pinnick RG, Wang RT. Scattering of electromagnetic waves by composite spherical particles: experiment and effective medium approximations. Appl Opt 1988;27:2396–404.
[8] Borghese F, Denti P, Saija R. Optical properties of spheres containing a spherical eccentric inclusion. J Opt Soc Am A 1992;9:1327–35.
[9] Videen G, Ngo D, Chýlek P, Pinnick RG. Light scattering from a sphere with an irregular inclusion. J Op. So. Am A 1995;12:922–8.
[10] Videen G, Chylek P. Scattering by a composite sphere with an absorbing inclusion and effective medium approximations. Opt Commun 1998;158:1–6.
[11] Chýlek P, Videen G, Ngo D. Effect of air bubbles on absorption of solar radiation by water droplets. J Atmos Sci 1998;55:340–3.
[12] Chýlek P, Videen G. Scattering by a composite sphere and effective medium approximations. Opt Commun 1998;146:15–20.
[13] Bohren CF. Applicability of effective medium theories to problems of scattering and absorption by nonhomogeneous atmospheric particles. J Atmos Sci 1986;43:468.
[14] Chýlek P, Srivastava V. Dielectric constant of a composite inhomogeneous medium. Phys Rev B 1983;27:5098–109.
[15] Chýlek P, Lesins GB, Videen G, Wong JGD, Pinnick RG, Ngo D, et al. Black carbon and absorption of solar radiation by clouds. J Geophys Res 1996;101:23365–71.
[16] Chýlek P, Videen G, Ngo D, Pinnick RG, Klett JD. Effect of black carbon on the optical properties and climate forcing of sulfate aerosols. J Geophys Res 1995;100:16325–6,332.
[17] Chýlek P, Ramaswamy V, Cheng RJ. Effect of graphitic carbon on the albedo of clouds. J Atmos Sci 1984;41:3076–84.
[18] Mishchenko MI, Liu L, Mackowski DW. Morphology-dependent resonances of spherical droplets with numerous microscopic inclusions. Opt Lett 2014;39:1701–4.
[19] Mackowski DW. A general superposition solution for electromagnetic scattering by multiple spherical domains of optically active media. J Quant Spectrosc Radiat Transf 2014;133:264–70.
[20] Borghese F, Denti P, Saija R. Optical properties of spheres containing several spherical inclusions. Appl Opt 1994;33:484–93.
[21] Mishchenko MI, Dlugach ZhM, Zakharova NT. Direct demonstration of the concept of unrestricted effective-medium approximation. Opt Lett 2014;39:3935–8.
[22] Purcell EM, Pennypacker CR. Scattering and absorption of light by nonspherical dielectric grains. Astrophys J 1973;186:705–14.
[23] Goodman JJ, Draine BT, Flatau PJ. Application of fast-Fourier-transform techniques to the discrete-dipole approximation. Opt Lett 1991;16:1198–200.
[24] Draine BT, Goodman JJ. Beyond Clausius–Mossotti: wave propagation on a polarizable point lattice and the discrete dipole approximation. Astrophys J 1993;405:685–97.
[25] Zubko E, Shkuratov Yu, Hart M, Eversole J, Videen G. Backscattering and negative polarization of agglomerate particles. Opt Lett 2003;28:1504–6.
[26] Penttilä A, Zubko E, Lumme K, Muinonen K, Yurkin MA, Draine B, et al. Comparison between discrete dipole implementations and exact techniques. J Quant Spectrosc Radiat Transf 2007;106:417–36.
[27] Zubko E, Kimura H, Shkuratov Yu, Muinonen K, Yamamoto T, Okamoto H, et al. Effect of absorption on light scattering by agglomerated debris particles. J Quant Spectrosc Radiat Transf 2009;110:1741–9.
[28] Zubko E, Muinonen K, Shkuratov Y, Videen G, Nousiainen T. Scattering of light by roughened Gaussian random particles. J Quant Spectrosc Radiat Transf 2007;106:604–15.
[29] Zubko E, Videen G, Shkuratov Y, Muinonen K, Yamamoto T. The Umov effect for single irregularly shaped particles with sizes comparable with wavelength. Icarus 2011;212:403–15.
[30] Warren SG. Optical constants of ice from the ultraviolet to the microwave. Appl Opt 1984;23:1206–25.
[31] Sun WB, Videen G, Kato S, Lin B, Lukashin C, Hu YX. A study of subvisual clouds and their radiation effect with a synergy of CERES, MODIS, CALIPSO, and AIRS data. J Geophys Res Atmos 2011;116:D22207.
[32] Sun W, Hu Y, Lin B, Zhaoyan Liu Z, Videen G. The impact of ice cloud particle microphysics on the uncertainty of ice water content retrievals. J Quant Spectrosc Radiat Transf 2011;112:189–96.
[33] Sun WB, Hu YX, Lin B, Liu ZY, Videen G. The impact of ice cloud particle microphysics on the uncertainty of ice water content retrievals. J Quant Spectrosc Radiat Transf 2011;112:189–96.
[34] Kimura H, Kolokolova L, Mann I. Optical properties of cometary dust. Constraints from numerical studies on light scattering by aggregate particles. Astron Astrophys 2003;407:L5–8.
[35] Lasue J, Levasseur-Regourd AC. Porous irregular aggregates of sub-micron sized grains to reproduce cometary dust light scattering observations. J Quant Spectrosc Radiat Transf 2006;100:220–36.
[36] Kolokolova L, Kimura H, Kiselev N, Rosenbush V. Two different evolutionary types of comets proved by polarimetric and infrared properties of their dust. Astron Astrophys 2007;463:1189–96.
[37] Jockers K. Observations of scattered light from cometary dust and their interpretation. Earth Moon Planets 1997;79:221–45.
[38] Zubko E, Muinonen K, Shkuratov Y, Videen G. Characteristics of cometary dust in the innermost coma derived from polarimetry by Giotto. Mon Notes R Astron Soc 2013;430:1118–24.
[39] Zubko E, Furusho R, Kawabata K, Yamamoto T, Muinonen K, Videen G. Interpretation of photo-polarimetric observations of comet 17P/Holmes. J Quant Spectrosc Radiat Transf 2011;112:1848–63.
[40] Duley WW. Refractive indices for amorphous carbon. Astrophys J 1984;287:694–6.
[41] Jenniskens P. Optical constants of organic refractory residue. Astron Astrophys 1993;274:653–61.
[42] Dorschner J, Begemann B, Henning T, Jaeger C, Mutschke H. Steps toward interstellar silicate mineralogy. II. Study of Mg–Fe–silicate glasses of variable composition. Astron Astrophys 1995;300:503–20.
[43] Mukai T, Mukai S, Kikuchi S. Complex refractive index of grain material deduced from the visible polarimetry of comet P/Halley. Astron Astrophys 1987;187:650–2.
[44] Maron N, Maron O. On the mixing rules for astrophysical inhomogeneous grains. Mon Notes R Astron Soc 2005;357:873–80.
[45] Voshchinnikov NV, Il'in VB, Henning Th. Modelling the optical properties of composite and porous interstellar grains. Astron Astrophys 2005;429:371–81.
[46] Chýlek P, Grams GW, Pinnick RG. Light scattering by irregular randomly oriented particles. Science 1976;6:480–2.